Journal of Alloys and Compounds 509 (2011) 2001–2006

Contents lists available at ScienceDirect

Journal of Alloys and Compounds

journal homepage: www.elsevier.com/locate/jallcom

Synthesis and characterizations of AgI nanoparticles via mechanochemical reaction

Nor Liza Hawari*, Mohd Rafie Johan

Advanced Materials Research Laboratory, Department of Mechanical Engineering, University of Malaya, Lembah Pantai, 50603 Kuala Lumpur, Malaysia

ARTICLE INFO

Article history:
Received 28 February 2010
Received in revised form 22 October 2010
Accepted 24 October 2010
Available online 3 November 2010

Keywords:
Mechanochemical technique
Superionic phase
Activation energy
Particle size
Phase transition

ABSTRACT

Silver iodide (AgI) nanoparticles were prepared by mechanochemical reaction technique (MCR) using silver nitrate ($AgNO_3$) and potassium iodide (KI) as reagents and distilled water as solvent. Mechanochemical reaction involves the mechanical activation of solid-state displacement reactions at low temperatures in a ball mill. AgI nanoparticles with well-defined morphology, size and phase compositions were obtained. TEM images show that the particle size of the AgI nanoparticles decreases as a function of milling time. The powder X-ray diffraction patterns show that they are mixture of γ- and β-phases. The superionic phase transition temperature ($\gamma \rightarrow \alpha$) was slightly decreased after milling. The ionic conductivity shows enhancement with temperature for all samples with the unmilled sample has the highest conductivity (4.12×10^{-6} S cm^{-1}) at room temperature. The growth kinetics for AgI nanoparticles were investigated. Two different values of activation energy were obtained indicated that there were two kind of mechanisms for the growth of AgI nanoparticles.

1. Introduction

Over the past few years, nanoparticles have been investigated extensively due to their novel properties that are greatly differ from the bulk materials [1–3]. Their defining characteristics is their size which is in the range of 1–100 nm and excellent chemical processability. Comparing nanoparticles with the bulk material, some different properties are expected, namely a lower melting point, a lower phase transition temperature, different electrical and magnetic properties, a higher catalytic activity, etc. Semiconductor nanoparticles such as silver iodide (AgI) attract special interest because they are in an intermediate state between atoms molecules and bulk materials and can be expected to exhibit excellent properties [4]. Investigations of AgI have prompted progress in the fields of solid state ionics and photography and applications of relevant devices. Thus, the design and controlled synthesis of nanostructures is very important [5–7]. Several approaches have been developed to synthesize AgI nanoparticles [8–11]. Recently, mechanochemical reaction (MCR) has emerged as a variable method to produce nanoscale materials [10]. This technique generally influences texture and structure leading to a decrease of the particle size and simultaneously increases the microstain due to the contribution of the grain boundaries formed during the process [11]. AgI is a remarkable compound due to its superionic α-phase and high Ag^+ conductivity [12]. AgI has a direct bandgap (~2.9 eV) and it usually is a mixture of β-AgI and γ-AgI at room temperature. Above 147 °C, AgI has the α-phase that shows the superionic behavior which have been studied extensively [13]. AgI is the most investigated superionic conductor. Its ionic conductivity was attributed to the highly disordered structure of the phase. Extensive efforts have been made to investigate the size dependence on the phase transition temperature and ionic conductivity [14,15]. In this paper, we report phase, conductivity and growth studies of AgI nanoparticles synthesized by simple MCR technique. An important goal of this study is to observe the effects of the particle size on the correlations between ionic conductivity, thermal events and phase transformations of the compound. We also investigated the formation and growth of AgI nanoparticles.

2. Experimental procedure

AgI nanoparticles were prepared from the reagents silver nitrate ($AgNO_3$) and potassium iodide (KI) using distilled water as solvent. Optimized preparation route for AgI nanoparticles are as follows. Two separate solutions containing $AgNO_3$ and KI were rapidly mixing. The mixtures were vigorously stirred for 15 min, filtered and left to dry for a day. The precipitates were collected, repeatedly washed with distilled water and then sintered at 250 °C for 5 h. Planetary ball mill was used to grinding the AgI powder for 40–70 h. Microstructural characterization was performed by Transmission electron microscopy and X-ray Diffraction (XRD) Philips X'pert MRD diffractometer with CuKα radiation (λ = 1.5056 Å). TEM samples were prepared by placing a drop of a dilute methanol suspension of AgI on the surface of a 300-mesh copper grid which was then dried for five days. TEM observations were carried out in a LEO 912 Omega operating at 120 kV. Pellets of AgI powders were prepared pressing the powder uniaxially at 5 ton into discs of diameter 25 mm with a thickness of 3.6 mm for electrical measurement. Conductivity studies were carried out

* Corresponding author.
E-mail address: norliza2613@yahoo.com (N.L. Hawari).

0925-8388/$ – see front matter © 2010 Elsevier B.V. All rights reserved.
doi:10.1016/j.jallcom.2010.10.116

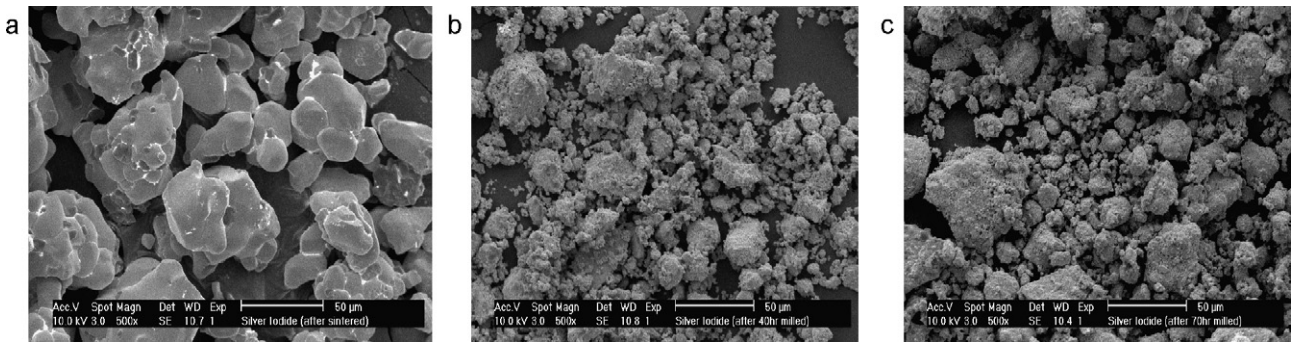

Fig. 1. SEM images of AgI powders: (a) non-milled; (b) 40 h milled; (c) 70 h milled.

using Impedans spectroscopy HIOKI 3532-50 LCR Hi Tester with frequency range of 50 Hz to 1 MHz. Thermal studies were carried out using METTLER 820 Differential Scanning Calorimetry.

3. Results and discussion

3.1. SEM analysis

Fig. 1 shows the typical SEM images of the AgI powders before and after milling.

Secondary electron images show qualitatively the differences in the surface morphology of mechanochemically reacted ground samples of AgI. Random orientation of bigger size crystallites were observed in the non-milled sample (Fig. 1(a)). However, the crystallite size clearly decreases after 40 h of milling time (Fig. 1(b)). As the milling time increases to 70 h, the crystallite size continuously decreased. Agglomerated crystallites with small size and increased reactive surface area were observed in the milled samples. Even though, the MCR technique is a non-equilibrium processing route, our SEM observation suggests that apart from incorporating residual strain, the samples obtained are largely homogeneous. The relatively low energy cost for and high efficiency of the process could lead to the homogeneous samples.

3.2. TEM analysis

Fig. 2 shows TEM images and particle size distribution of the AgI powders before and after milling.

Spherical shape and well dispersed of AgI nanoparticles were observed for unmilled sample as shown in Fig. 2(a). The average particle size of non-milled AgI nanoparticles is 50 nm. The shape and distribution are well maintained after milling for 40 h. However, the average particle size decreases to 20 nm as shown in Fig. 2(d). Particles start to agglomerate and become a cluster after milling for 70 h (Fig. 2(e)) with the average particle size of 10 nm.

3.3. XRD analysis

Fig. 3 shows the XRD patterns of unmilled, 40 and 70 h milled samples.

It is well known that AgI crystals consist of hexagonal wurtzite-type β-AgI and cubic zinc blende-type γ-AgI under ambient condition as clearly seen in the figure. In the long condition of investigations of AgI, many synthetic methods have been studied for the preparation of AgI nanoparticles and it difficulty is to obtain pure crystals of a single phase. The unmilled sample exhibits a mixture of two phases, β-AgI and γ-AgI from small angle of 22° until 70°. However, most of peaks at large angle were disappeared after milling the sample for 40–70 h. Nevertheless, the milled samples still con-

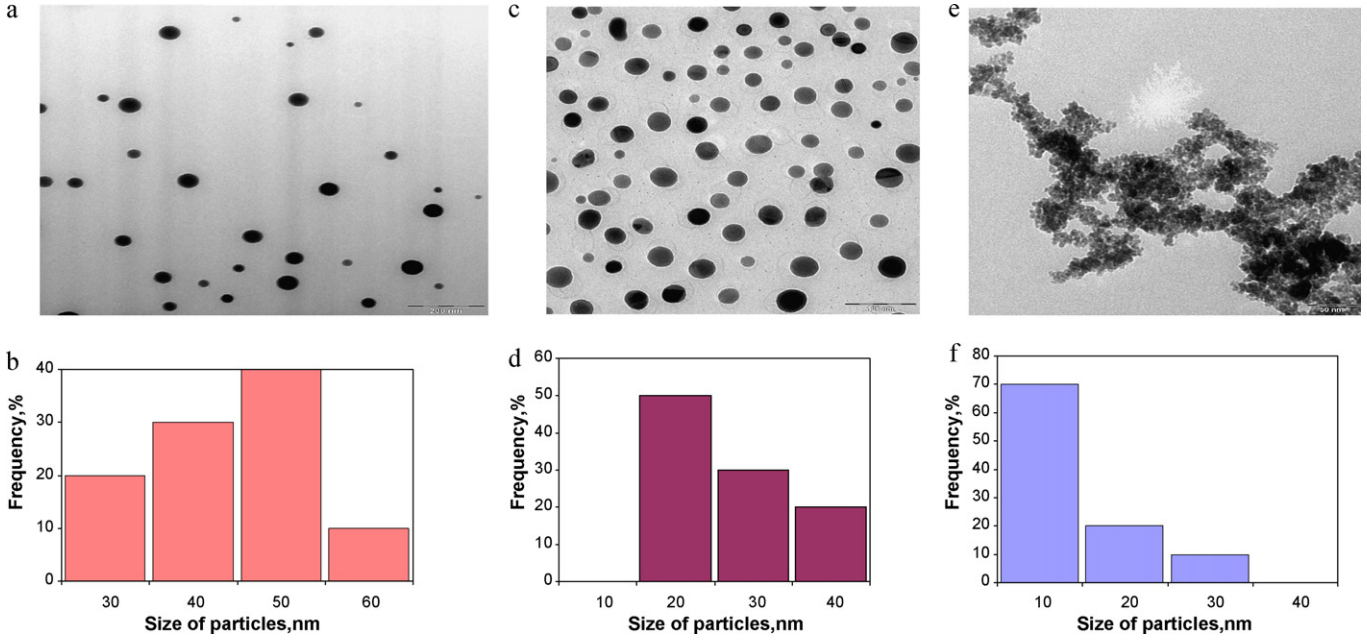

Fig. 2. TEM images and size distribution of AgI nanoparticles: (a–b) non-milled; (c–d) after 40 h milled; (e–f) after 70 h milled.

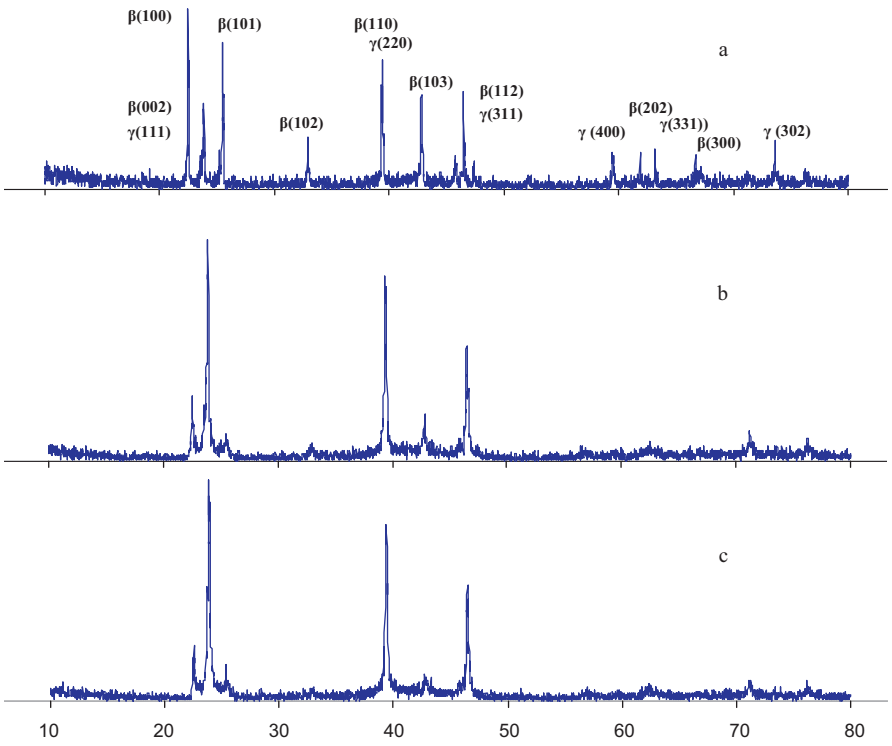

Fig. 3. XRD pattern of AgI samples: (a) non-milled; (b) 40 h milled; (c) 70 h milled.

sist a mixture of two phases β-AgI and γ-AgI. It was also found that the FWHM (full width at half maximum) increases after milling. The increase of FWHM is evidence of decreases in AgI crystallite size. The crystallite size of the samples are calculated through Scherrer's formula in Eq. (1)

$$s = \frac{k\lambda}{\beta \cos\theta} \quad (1)$$

where k is a Scherrer constant, λ is a X-ray wavelength, β is a full width at half maximum (FWHM) and θ is a peak angle. Table 1 shows the crystallite size of the samples decreases as the milling time increases. Note that the FWHM value was obtained from the peak at angle of 24°.

3.4. DSC analysis

Fig. 4 shows the thermal response of the AgI powders before and after milling.

It seen that DSC traces of the heating runs consist of a strong single endotheric peak near 147 °C due to the order–disorder phase transition of AgI from the low temperature β/α-phase to superionic high temperature α-phase. The endothermic was observed to decrease slightly with the decrease of the AgI particle diameter. With restricting the particle size to be in nm-order, the phase transition temperature of the AgI particle might be lower than that of the bulk AgI and the high-temperature phase of α-AgI will possibly be brought to room temperature making AgI as a valuable material for solid-state battery, solid sensor, and others.

Table 1
FWHM and crystallite size of AgI samples before and after milling.

Sample	FWHM ($\times 10^{-3}$ rad)	Crystallite size (nm)
Before milling	5.24	26.9
40 h milled	6.98	20.2
70 h milled	8.72	16.2

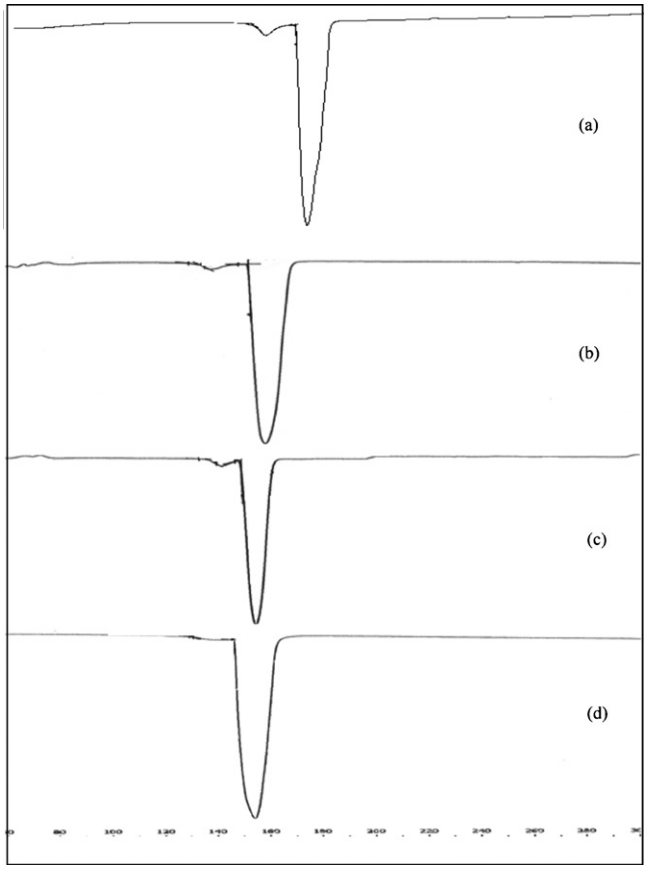

Fig. 4. DSC traces of AgI samples: (a) bulk AgI; (b) before milled; (c) after 40 h milled; (d) after 70 h milled.

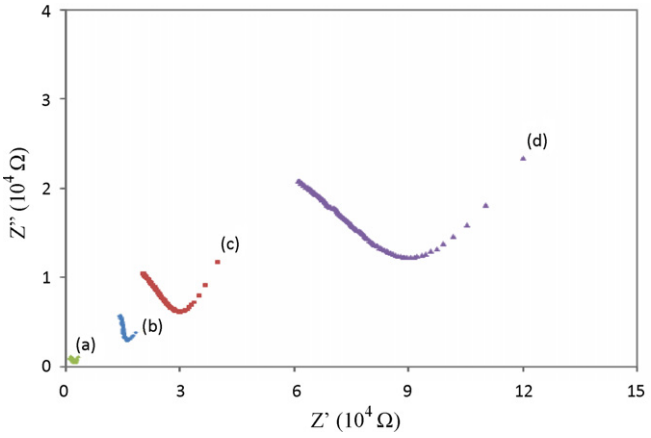

Fig. 5. . Room temperature impedance plots for samples of (a) 70 h milled; (b) 40 h milled; (c) unmilled; (d) bulk AgI.

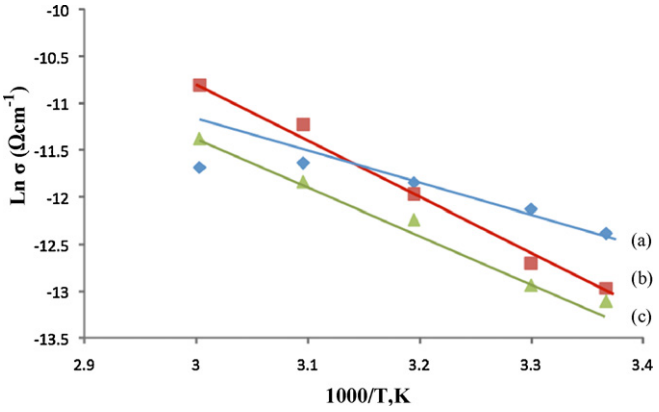

Fig. 6. Temperature dependence of the ionic conductivity for (a) unmilled; (b) 40 h milled; (c) 70 h milled AgI samples.

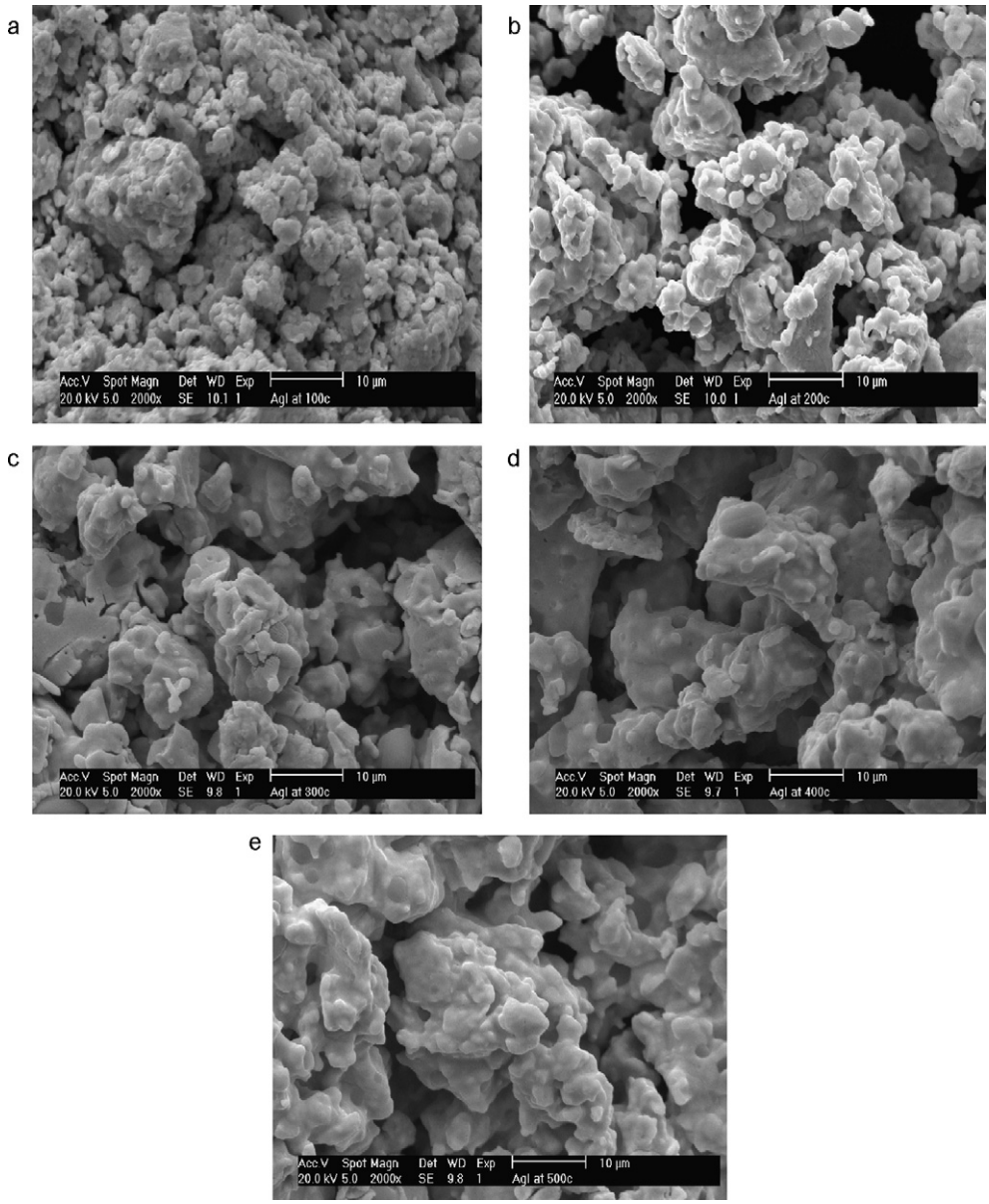

Fig. 7. SEM images of the AgI nanoparticles at 70 h milling time for various sintering temperatures: (a) 100 °C; (b) 200 °C; (c) 300 °C; (d) 400 °C; (e) 500 °C.

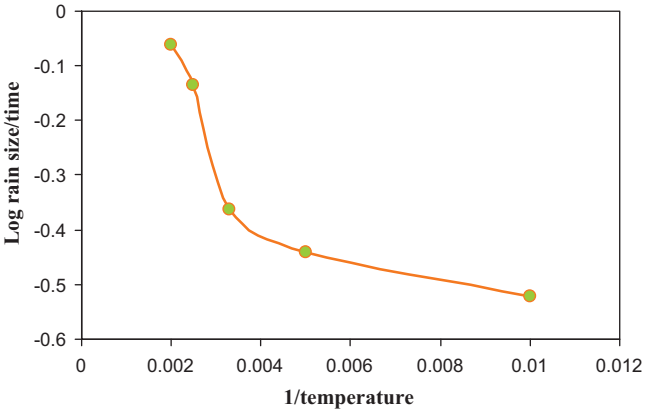

Fig. 8. Plot of log grain/time versus inverse temperature of 70 h milled AgI.

3.5. Complex impedance studies

Impedance plane plots of the samples are presented in Fig. 5. All samples show spike at lower frequency and small part of semicircle at higher frequencies. The spike is related to the interfacial effects between the electrode and samples while the semicircle can be attributed to the bulk resistance of the samples assuming the grain boundary effect to be the minor. The diameter of semicircle was observed to decrease with the decrease of the AgI particle diameter. The DC resistivity can be obtained from the intersection of the semicircle which represents the bulk contribution with the axis of the real impedance decreasing rapidly with the decreasing particle size which indicates increasing ionic conductivity. The ionic conductivity can be calculated from the equation below:

$$\sigma = \frac{t}{R_b A} \tag{2}$$

where R_b, t and A are the bulk resistance, thickness and cross sectional area of the sample, respectively.

3.6. Temperature dependence of ionic conductivity

Temperature dependence of the ionic conductivity for the AgI samples was investigated by complex impedance measurement as presented in Fig. 6. With the particle size decreasing, the RT ionic conductivity decreases from 4.12×10^{-6} to 2.02×10^{-6} S cm^{-1}. Fig. 6 composed of three linear plots which can be fitted by Arrhenius equation,

$$\sigma = \sigma_o \exp\left(-\frac{E_A}{k_B T}\right) \tag{3}$$

where σ_o is the pre-exponential factor, k_B represents the Boltzmann constant and E_A is the activation energy. The activation energies for the three plots of Fig. 6 were calculated to be 0.17, 0.26 and 0.35 eV, respectively. It has been well established [16] that the ionic conductive behavior of normal AgI below 147 °C is controlled by extrinsic defects in the lattice, such as grain boundaries and dislocations. However, the mechanism of ionic conductivity for nano-AgI was seldom studied. At temperatures ranging from RT to 147 °C, we proposed that the conductive mechanism of both normal and nano-AgI is the same. The increase in ionic conductivity and decrease in activation energy may result from the increase of grain boundary and dislocation density in AgI nanoparticles which can provide a high diffusivity path for Ag at low temperatures.

3.7. Growth study

Fig. 7 shows the SEM micrographs of the AgI samples sintered for 5 h at different temperatures.

The particles are well distributed at the beginning of sintering process as shown in Fig. 7(a). The porosity among the particles is less visible. As the temperature gradually increases at 200 °C, the particles tend to agglomerate to form a cluster. Porosity among the particles is more visible. A similar feature occurred at the higher temperatures. The particle size was grown and become more dense and compact. In order to give a better understanding of the grain growth behavior during sintering, an analysis of the kinetic grain growth is carried out based on the kinetic grain growth equation:

$$G = k_o t \exp\left[\frac{-E}{RT}\right] \tag{4}$$

where G is grain size, k_o is constant, t is a time, E is an activation energy and R is a universal gas constant.

Fig. 8 shows the grain size as a function of temperature. As shown in the figure, the grain size increases gradually with increasing temperature in the low temperature region. Sudden increases in grain size are observed at 300 °C. This rise in grain size is accompanied by higher activation energy. In the low temperature region, the activation energy was 20 kJ/mol. In the high temperature region, the rate was faster and the activation energy was 400 kJ/mol. The higher activation energy for the high temperature phase can be explained by the presence of structural disorder in these compounds. We proposed that there are two different mechanisms for grain growth at lower and higher temperature as reflected from two different values of the activation energy.

4. Conclusion

The AgI nanoparticles were prepared using a simple mechanochemical route and then sintered at 500 °C for growth study. It was found that the size of AgI nanoparticles decreases as a function of the milling time. The AgI nanoparticles become homogeneous during mechanical milling. The morphological changes are followed by structural changes. Most of the XRD peaks at a large angle were disappeared after milling even though they still consist a mixture of two phases β-AgI and γ-AgI. The DSC study shows that the phase transition temperature ($\gamma \rightarrow \alpha$) slightly decreases after milling. Ionic conductivity study shows a thermal dependence conductivity which satisfied the Arrhenius profile. The conductivity is due to the grain boundaries and dislocations. In addition, we proposed that there would be two different mechanisms for the grain growth as reflected from two different values of the activation energy.

Acknowledgments

The financial support received from Science fund (13-02-03-3068) Ministry of Science, Technology and Innovation Malaysia is gratefully acknowledged.

References

[1] B. Gates, Y. Yin, Y. Xia, J. Am. Chem. Soc. 122 (2000) 12582.
[2] Y. Dongzhi, C. Qifan, X. Shukun, J. Lumin. 126 (2007) 853.
[3] X.G. Peng, J. Wickham, A.P. Alivisatos, J. Am. Chem. Soc. 120 (1998) 5343.
[4] K. Kimura, Z. Phys. D 11 (1989) 327.
[5] H.T. Shi, L.M. Qi, J.M. Ma, H.M. Cheng, J. Am. Chem. Soc. 125 (2003) 3450.
[6] H. Zhang, D.R. Yang, D.S. Li, X.Y. Ma, S.Z. Li, D.L. Que, J. Cryst. Growth 5 (2005) 547.
[7] B.D. Kuang, A.W. Xu, Y.P. Fang, H.Q. Lin, C. Frommen, D. Fenske, Adv. Mater. 15 (2003) 1747.
[8] A.R. Abbosi, A. Morsali, Ultrason. Sonochem. 17 (2010) 577.

[9] T. Ida, K. Kimura, Sol. Stat. Ion 107 (1998) 313.
[10] Y.H. Wang, J.M. Mo, W.L. Cai, L.Z. Yao, J. Mater. Res. 16 (2001) 990.
[11] Y.X. Wang, L. Huang, H.P. He, M. Li, Physica B 325 (2003) 357.
[12] S. Chandra, Superionic Solids: Principles and Application, North Holland, Amsterdam, 1991.
[13] S.V. Baryshnikov, et al., J. Phys. Condens. Matter 20 (2008) 025214.
[14] M. Hanaya, I. Osawa, K.J. Watanabe, Therm. Anal. Cal. 76 (2004) 529–536.
[15] R. Makiura, et al., Nat. Mater. 8 (2009) 476–480.
[16] R.J. Cava, E.A. Rietman, Phys. Rev. B 30 (12) (1984) 6896.